3D Mapping Database Aided GNSS Based Collaborative Positioning Using Factor Graph Optimization

Guohao Zhang, Hoi-Fung Ng, Weisong Wen, and Li-Ta Hsu, *Member, IEEE*

***Abstract*— The recent development in vehicle-to-everything (V2X) communication opens a new opportunity to improve the positioning performance of the road users. We explore the benefit of connecting the raw data of the global navigation satellite system (GNSS) from the agents. In urban areas, GNSS positioning is highly degraded due to signal blockage and reflection. 3D building model can play a major role in mitigating the GNSS multipath and non-line-of-sight (NLOS) effects. To combine the benefits of 3D models and V2X, we propose a novel 3D mapping aided (3DMA) GNSS-based collaborative positioning method that makes use of the available surrounding GNSS receivers' measurements. By complementarily integrating the ray-tracing based 3DMA GNSS and the double difference technique, the random errors (such as multipath and NLOS) are mitigated while eliminating the systematic errors (such as atmospheric delay and satellite clock/orbit biases) between road user. To improve the accuracy and robustness of the collaborative algorithm, factor graph optimization (FGO) is employed to optimize the positioning solutions among agents. Multiple low-cost GNSS receivers are used to collect both static and dynamic data in Hong Kong and to evaluate the proposed algorithm by post-processing. We reduce the GNSS positioning error from over 30 meters to less than 10 meters for road users in a deep urban canyon.**

***Index Terms*— GNSS, collaborative positioning, 3D building model, ray-tracing, V2X, NLOS, urban canyon.**

I. Introduction

DUE to the rapid development of signal communication, information sharing between neighboring road users is becoming possible2. Researchers studied the new potentials by combining the measurements from the agents rather than only using the on-board measurements of one road user [1], [2]. Combined measurements can also improve the perception range of their surroundings or anti-spoofing ability [3], thereby contributing to road safety in intelligent transportation systems (ITS). Transponder-based methods are applied in vehicle-to-vehicle (V2V) collaborative positioning [4]–[6]. They use the time-of-arrival to measure the relative positions of different vehicles. However, these transponder-based methods suffer from non-line-of-sight issue (NLOS) [1] and are unable to obtain the relative distances from others when an obstacle is in-between two vehicles. Therefore, the detection ranges of these methods are limited. In contrast, the GNSS-based collaborative positioning method is able to overcome this issue and obtain full 3D relative position, even when obstacles exist in-between vehicles. Based on the shared GNSS measurements and the spatial relationships, the relative distances between different road agents can be estimated [7]. By applying the double difference (DD) on the shared GNSS raw measurements, the correlated errors including satellite orbit/clock biases, ionospheric and tropospheric delays, can be eliminated [8], [9] and obtain relative position between two road agents. The performance and limitation of the double difference GNSS based collaborative positioning method are evaluated with the Cramer-Rao lower bound (CRLB) [10].The relative positions of different vehicles are combined with absolute positions to optimize the position of the participated vehicles [11]. Moreover, the feasibility and improvements of integrating the inter-agent distances with GNSS measurements in a tightly-coupled architecture are studied [12]. However, the benefits of DD are limited to open-sky areas without NLOS or multipath effect [13], [14]. Unfortunately, GNSS receivers suffer from severe multipath and non-line-of-sight (NLOS) effects in urban areas [15]. The effects are strongly dependent on location. In other words, it cannot be eliminated or even mitigated by double differencing the measurements of road users. Since the multipath effect and NLOS reception are the dominant errors in urban areas [16], various algorithms are developed. A straightforward method is to integrate the GNSS with other sensors, which can maintain the positioning accuracy when GNSS measurements are not reliable. GNSS/INS integration has been widely applied to achieve robust positioning solutions [17]–[19]. Whereas, INS suffers from a continuous drift and is unable to guarantee the accuracy over long-time in dense urban areas without a reliable GNSS solution. Another approach is aiding GNSS with anchor-based measurements, for example, angle-of-arrival measurements [20], magnetic field strength [21], cellular signals [22], or more generally, the signals of opportunity [23]. However, the integration with other sensors requires additional hardware or infrastructures, as well as the consideration of the reliability of other sensors.

Since the multipath effects are caused by building reflections, researchers are studying the employment of 3D building

Manuscript received June 12, 2019; revised November 17, 2019 and February 18, 2020; accepted April 13, 2020. Date of publication April 30, 2020; date of current version October 4, 2021. This work was supported in part by the Shenzhen Municipal Science and Technology Innovation Committee on the Project under Grant JCYJ20170818103653507 and in part by The Hong Kong Polytechnic University Startup Fund on Project ZVKZ "Positioning and Navigation for Autonomous Driving Vehicle by Sensor Integration." The Associate Editor for this article was B. Fidan. *(Corresponding author: Li-Ta Hsu.)*

The authors are with the Interdisciplinary Division of Aeronautical and Aviation Engineering, The Hong Kong Polytechnic University, Hong Kong (e-mail: lt.hsu@polyu.edu.hk).

Digital Object Identifier 10.1109/TITS.2020.2988531

1558-0016 © 2020 IEEE. Personal use is permitted, but republication/redistribution requires IEEE permission.
See https://www.ieee.org/publications/rights/index.html for more information.

Authorized licensed use limited to: Hong Kong Polytechnic University. Downloaded on July 27,2023 at 10:24:04 UTC from IEEE Xplore. Restrictions apply.

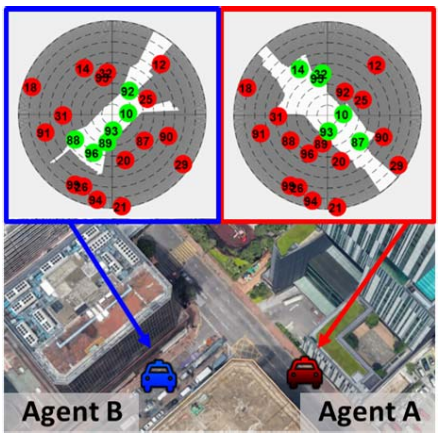

Fig. 1. Demonstration of the commonly-received GNSS measurements between different users in deep urban canyon. In the skyplots, green and red dots denote LOS and NLOS signals, respectively. Grey area denotes the area blocked by buildings.

models to mitigate these effects, as known as the 3D mapping-aided (3DMA) GNSS [24]–[30]. GNSS shadow matching (SDM) is one of the most widely applied 3DMA GNSS [31]–[33]. The detail and performance assessment of the state-of-the-art of 3DMA GNSS is reported in [24], [34]. A decentralized collaborative localization makes use of SDM and inter-agent ranging provided by ultra-wideband (UWB) is proposed and evaluated based on simulation [35]. The building model is also used to correct the UWB signal transmission delay when passing through walls, in order to improve the indoor collaborative positioning performance [36]. We previously proposed a pure 3DMA GNSS based collaborative positioning method. We used the SDM estimated satellite visibility to exclude the measurements affected by NLOS receptions before their use in double difference, thereby improving GNSS-based collaborative positioning in an urban area [37]. The experiment shows the previously proposed method can obtain satisfactory results if the number of common measurements between two road users is sufficient. However, the number of common line-of-sight (LOS) measurements are usually limited in deep urban canyons. An example is given in Fig.1. If most of NLOS are excluded, the reminding common measurements became few. Out of the 6 LOS signals for each user, only 2 LOS signals (10 and 93) are simultaneously visible for these users due to the different surrounding buildings (grey area). This insufficiency makes the GNSS relative positioning difficult. The reason is the exclusion will lead to the distortion of GNSS dilution of precision (DOP), resulting in poor positioning performance, which we experienced in our previous work [38].

Ray-tracing based 3DMA GNSS is developed to correct the multipath and NLOS errors from reflections [25], [27], [39]. Based on the pure reflection assumption, the reflected GNSS signal route can be simulated from the surfaces of buildings [40]. The extra traveling distance of the reflected GNSS signal can be estimated and used to correct the pseudorange measurements. Therefore, the ray-tracing algorithm is complementary to the GNSS based collaborative positioning in urban areas.

The aim of collaborative positioning is to improve the positioning accuracy of the road agents by centralizing and optimizing the absolute and relative positioning solutions provided by all participants. A study shows the effectiveness of using maximum likelihood estimation (MLE) [41]. However, the MLE may fail due to the nonconvex cost function. A convex relaxation is applied to solve the problem [42]. A cooperative method based on the least square is also developed to solve the non-convexity [43]. Multidimensional scaling (MDS) is another popular technique for collaborative positioning, exploring the spatial proximities between different agents with fast response [44], [45]. Recently, the factor graph optimization (FGO) is developed for applications with a large number of constraints [46], such as simultaneous localization and mapping (SLAM). FGO is well-known for its robustness against outliers [47]. It is also used in GNSS positioning under urban environments. The relate works show its ability in mitigating the outliers due to the multipath effect [48] and its potentials to outperform the extended Kalman filter (EKF) [49]. Thus, it is promising to apply FGO to GNSS based collaborative positioning.

This paper proposes a ray-tracing 3DMA GNSS based collaborative positioning using FGO. We aim to improve the positioning accuracy of road users in dense urban areas by this centralized method. First, the ray-tracing algorithm is used to correct the NLOS pseudorange error for individual agent. Then, the GNSS systematic errors are eliminated using the double difference technique, thereby obtaining relative positions between different agents. The graph of FGO is described by connecting the nodes (agents' state) based on the absolute and relative positions estimated by 3DMA GNSS and DD positioning, respectively. The reliability of each node and constraints are given by a predicted GNSS positioning error map [50]. The contributions of this paper are summarized as following: 1) Complementarily integrating the DD GNSS based collaborative positioning method with the ray-tracing based 3DMA GNSS to directly improve the GNSS positioning performance without the use of any additional sensors; 2) employing the factor graph optimization to obtain robust performance in dense urban areas, where outliers frequently occur.

The remainder of this paper is organized as follows. The overview of the proposed method is given in Section 2. The proposed grid-based 3DMA relative positioning with double difference technique is detailed in Section 3. In Section 4, the process of the factor graph optimization to achieve overall optimal positioning solution is introduced. The uncertainty of each constraint based on the predicted positioning error map is also introduced. After that, the improvement of the proposed algorithm is verified and discussed with real experiments in Section 5. Finally, the conclusion is drawn and future work is suggested in Section 6.

II. Overview of the Proposed Algorithm

The use of 3D mapping database to support the proposed 3DMA GNSS collaborative positioning is shown in Fig. 2. First, a set of grids is defined on the ground surface based

Authorized licensed use limited to: Hong Kong Polytechnic University. Downloaded on July 27,2023 at 10:24:04 UTC from IEEE Xplore. Restrictions apply.

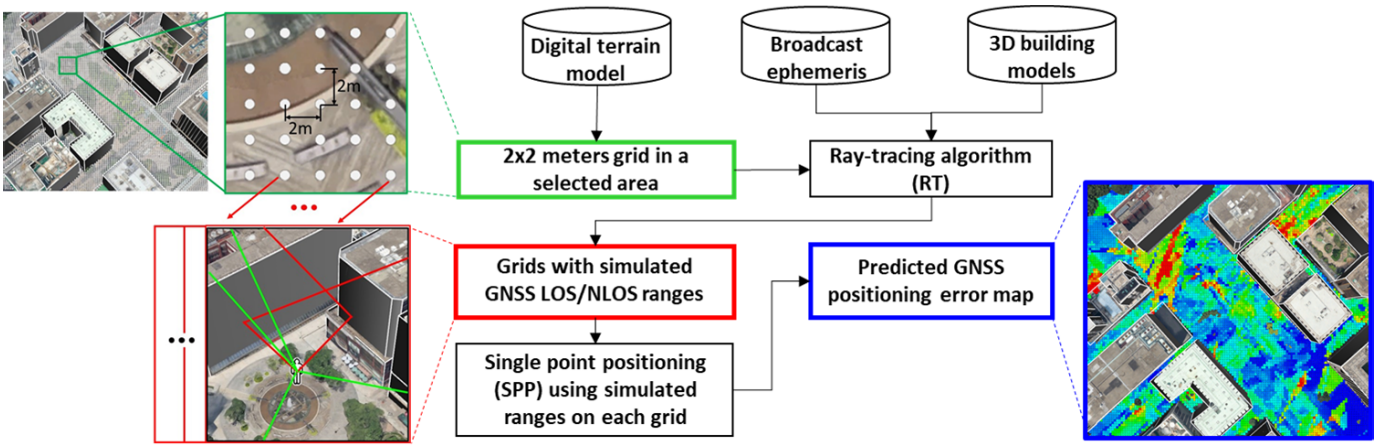

Fig. 2. The use of 3D mapping database in center server to generate simulated GNSS LOS/NLOS ranges from satellites to each grid and predicted GNSS positioning error map.

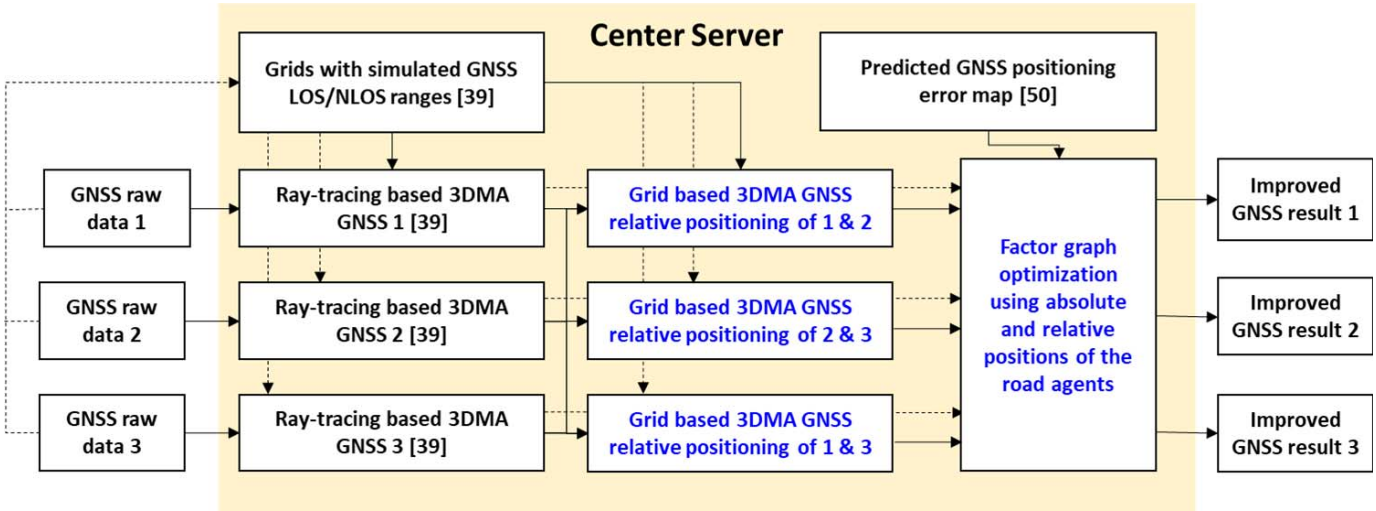

Fig. 3. The overview of the proposed 3DMA cooperative positioning with factor graph optimization. This is an example of 3 road agents participated in the collaborative positioning. The blue parts are the methods proposed in this paper. The parts highlighted in yellow are algorithms in the center server.

on digital terrain model (DTM) with a resolution of 2 by 2 meters in a selected area. The ray-tracing algorithm is used to simulate the GNSS LOS/NLOS ranges from satellites to each grid [39], which will be used in the 3DMA GNSS of the proposed collaborative positioning. In addition, the simulated ranges are used to predict the GNSS positioning error on each grid in the given time [50]. The system overview of the proposed 3DMA GNSS based collaborative positioning algorithm is given in Fig. 3. As shown in Fig.3, the road agents send their own GNSS raw data to the center server to conduct the proposed collaborative method. First, the ray-tracing based 3DMA GNSS algorithm [39] is applied to obtain the improved absolute position of individual road agents. In order to obtain an accurate relative position between two road agents, we propose a grid based 3DMA GNSS relative positioning method. The idea is similar to the previous work in [39]. Instead of comparing the pseudorange likelihood, the likelihood of the double difference measurements is considered. The detail will be introduced in the next section. After obtaining the absolute and relative positions, all these solutions are used as constraints for the factor graph optimization. Based on each agent's absolute position estimation, the corresponding positioning error can be evaluated by the predicted GNSS positioning error map and further used to obtain the uncertainty of the related constraint in the factor graph. Finally, by applying the factor graph optimization, the global optimal positioning of the participated road agents can be achieved with higher accuracy and robustness.

III. Grid Based 3DMA GNSS Relative Positioning

Conventionally, the relative position between two road agents can be estimated by double differencing the GNSS pseudorange measurements [51]. The problem is the multipath and NLOS affected measurements cannot be canceled or even mitigated during DD. Thus, the delay caused by reflections must be corrected before it is used in DD. Since the true position of the road agent is unknown, it is unable to derive the unique multipath and NLOS pseudorange corrections using the ray-tracing algorithm. A feasible approach is to select a number of grids near the initial position of the road agent. The initial position is given by the ray-tracing based 3DMA

Authorized licensed use limited to: Hong Kong Polytechnic University. Downloaded on July 27,2023 at 10:24:04 UTC from IEEE Xplore. Restrictions apply.

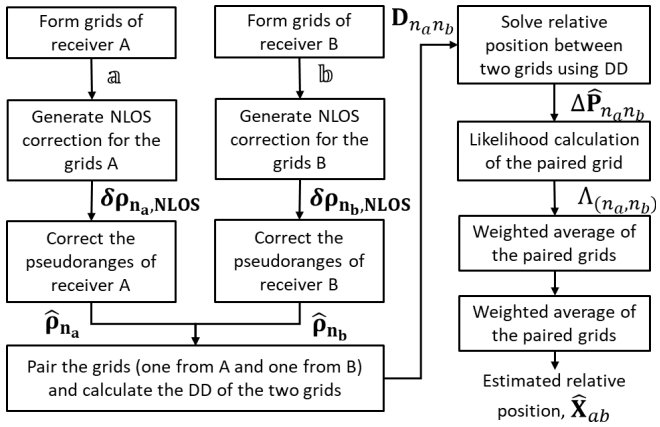

Fig. 4. The flowchart of the proposed grid based 3DMA GNSS relative positioning method.

GNSS [39]. By extending the idea of the ray-tracing based method, we propose to calculate the relative position based on a position hypothesis based method. Its flowchart is given in Fig.4.

Sets of grids $\mathbb{a}$ and $\mathbb{b}$ are selected for road agents a and b, respectively. Note that the height of the grids is given by DTM, assuming that the road agents are on the ground. If the ray-traced range of a grid is NLOS, then the NLOS correction of that particular grid can be calculated as:

$$\delta\rho^i_{n,NLOS} = L^i_n - R^i_n \tag{1}$$

where $\delta\rho^i_{n,NLOS}$ is the NLOS correction for the pseudorange from the ith satellite to the nth grid, L^i_n is the total distance of the simulated reflection path and R^i_n is the geometric LOS range between the nth grid and the ith satellite. Note that, the NLOS correction generated by ray-tracing is unique for each grid. The corrected range in a grid selected by road agent a is calculated as:

$$\hat{\rho}^i_{n_a} = \tilde{\rho}^i_a - \delta\rho^i_{n_a,NLOS} \tag{2}$$

where $\tilde{\rho}^i_a$ is the received pseudorange measurement from satellite i to road agent a. A grid closer to the true position of the road agent is more likely to obtain a correct correction. To estimate the relative position between two road agents, DD of the corrected range measurements is used. Like DGNSS, the road agents applying DD are better to be close within 1 km, ensuring the GNSS atmospheric delays are similar [52]. The calculation of the DD range between two grids selected by road agent a and b is as below:

$$D^{im}_{n_a n_b} = \left(\hat{\rho}^m_{n_b} - \hat{\rho}^i_{n_b}\right) - \left(\hat{\rho}^m_{n_a} - \hat{\rho}^i_{n_a}\right) \tag{3}$$

where the superscript m denotes the master satellite. We selected the satellite with the highest elevation angle as the master satellite in this paper. Due to the distance between satellite and road agent is far way comparing to the distance between two road agents, their relationship can be linearized as following [52]:

$$D^{im}_{n_a n_b} = \left(\vec{\eta}^m - \vec{\eta}^i\right) \cdot \Delta\hat{\mathbf{P}}_{n_a n_b} \tag{4}$$

where $\vec{\eta}^i$ and $\vec{\eta}^m$ are the unit line-of-sight (LOS) vectors

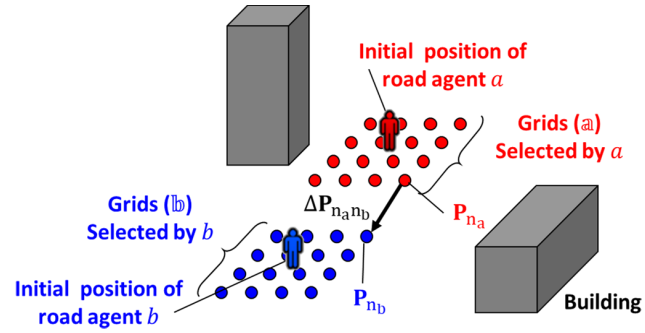

Fig. 5. The demonstration of the grids selected by two road agents.

from the road agent to satellites i and m, respectively. $\Delta\hat{\mathbf{P}}_{n_a n_b}$ denotes the relative position between the grids n_a and n_b selected by road agent a and b, respectively. It is demonstrated in Fig. 5. Equation (4) can be re-written as:

$$D^{im}_{n_a n_b} = \mathrm{A}^{im}\,\Delta\hat{\mathbf{P}}_{n_a n_b} \tag{5}$$

Considering the DD ranges from different satellites, the relative position can be solved by pseudo-inversing matrix $\mathbf{A}$:

$$\Delta\hat{\mathbf{P}}_{n_a n_b} = \left(\mathbf{A}^{\mathbf{T}}\mathbf{A}\right)^{-1}\mathbf{A}^{\mathbf{T}}\mathbf{D}_{n_a n_b} \tag{6}$$

We assume if both selected grids are close to the real position of road agents, the corresponding estimated relative position, $\Delta\hat{\mathbf{P}}_{n_a n_b}$, should be closer to the true relative position between road agents a and b. In contrast, if both of the grids are far away from the real road agent positions, the ray-tracing correction will be incorrect. Using the faulty corrections will increase the uncommon errors in DD range, resulting in the corresponding relative positioning error will be largely increased. As a result, the estimated relative position with faulty corrections will be very different from the actual relative position between the two grids. The difference is calculated as:

$$\delta\Delta\mathbf{P}_{(n_a,n_b)} = \left\|\left(\mathbf{P}_{n_b} - \mathbf{P}_{n_a}\right) - \Delta\hat{\mathbf{P}}_{n_a n_b}\right\| \tag{7}$$

If the assumption is valid, the likelihood (the posterior probability) of each pair of grids can be estimated using the difference as following:

$$\Lambda_{(n_a,n_b)} = exp\left[\frac{\left(\delta\Delta\mathbf{P}_{(n_a,n_b)} - \delta\Delta\mathbf{P}_{min}\right)}{\left(\delta\Delta\mathbf{P}_{max} - \delta\Delta\mathbf{P}_{min}\right)}\right]^{-1} \tag{8}$$

$$\delta\Delta\mathbf{P}_{min} = \min_{n_a\in\mathbb{a},n_b\in\mathbb{b}}\left\{\delta\Delta\mathbf{P}_{(n_a,n_b)}\right\} \tag{9}$$

$$\delta\Delta\mathbf{P}_{max} = \max_{n_a\in\mathbb{a},n_b\in\mathbb{b}}\left\{\delta\Delta\mathbf{P}_{(n_a,n_b)}\right\} \tag{10}$$

where $\Lambda_{(n_a,n_b)}$ is the estimated likelihood of the paired grids n_a and n_b. The total set of different combining pairs of the grid selected from road agents a and b can be expressed as:

$$\mathbf{Pair} = \{(n_a, n_b) \mid n_a \in \mathbb{a}, n_b \in \mathbb{b}\} \tag{11}$$

$\delta\Delta\mathbf{P}_{min}$ and $\delta\Delta\mathbf{P}_{max}$ are the minimum and maximum of the calculated differences of all the pairs. We normalized the difference $\delta\Delta\mathbf{P}_{(n_a,n_b)}$ and prioritized the pairs based on the likelihood. The larger likelihood of the pair (smaller difference) is, the higher chance the pair can reflect the actual

Authorized licensed use limited to: Hong Kong Polytechnic University. Downloaded on July 27,2023 at 10:24:04 UTC from IEEE Xplore. Restrictions apply.

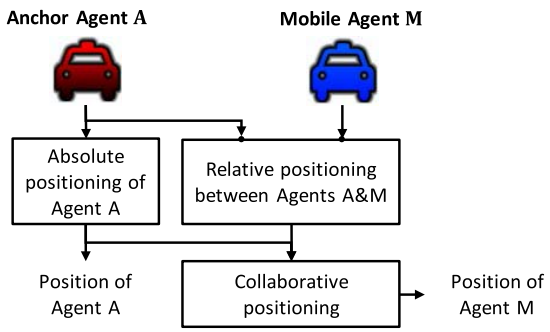

Fig. 6. The concept of the anchor-based GNSS collaborative positioning method.

relative position of the road agents. To gain robustness of the proposed method, we selected (filtered) the top 1% of all the pairs in this study. For example, if 100 grids are selected by each road agent, 10,000 pairs are generated between two road agents. Then, 1% means 100 pairs. Finally, the relative position between road agents a and b can be determined by weighted average of all the filtered pairs (denoted as $\mathbf{Pair}^*$ and $pair^*$ for a subset).

$$\Delta\hat{\mathbf{x}}_{ab} = \left(\sum\nolimits_{\mathbf{Pair}^*} \Lambda_{pair^*} \cdot \Delta\mathbf{P}_{pair^*}\right) \Big/ \sum\nolimits_{\mathbf{Pair}^*} \Lambda_{pair^*} \quad (12)$$

By applying the proposed 3DMA GNSS relative positioning method, an accurate relative position can be estimated even when two road agents are located in urban canyons. The relative positions of all the combinations of the road agents are estimated using the proposed method.

IV. Factor Graph Optimization Based Collabotative Positioning

If a road agent is identified driving in GNSS friendly areas, the agent can play the role of "anchor" in the collaborative positioning [37]. As the demonstration in Fig. 6, by collaborating the healthy measurement from the anchor agent, the nearby mobile agent is able to obtain a better positioning solution. However, it is always difficult to correctly identify the "anchor" in the system. In other words, it is not robust. Instead of using an anchor, we should consider collaborative positioning as a problem of optimization. The absolute position of agents (calculated by ray-tracing based method) and the relative positions between agents (calculated by the proposed grid based 3DMA GNSS relative positioning) are regarded as constraints in the optimization process.

Since the number of constraints becomes enormous when more road agents are participating, the factor graph optimization (FGO) becomes a good candidate to conduct collaborative positioning. FGO is famous for its outstanding performance with a large number of constraints [47]. Since we assume the road agents are driving or walking on the ground, we focus on the positioning in the East-North (horizontal) plane of the local coordinate. In this study, the FGO is based on the open source toolbox (gtsam-toolbox-3.2.0) [46].

A. Factor Graph Construction

The factor graph (including nodes and edges) of the proposed collaborative positioning system can be defined as shown in Fig. 7.

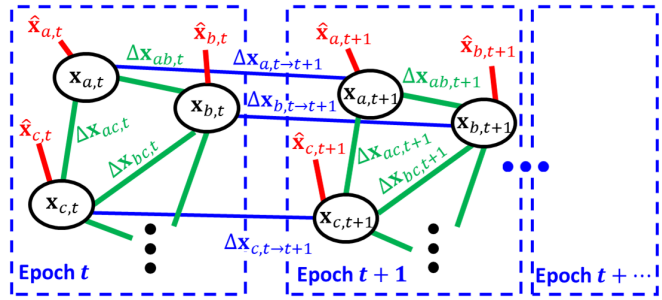

Fig. 7. The proposed factor graph for the 3DMA GNSS-based collaborative positioning system. Node is denoted as a black circle. Lines (edges) with different colors denote different types of constraints, including 3DMA GNSS absolute positioning (red) and relative positioning (green) and GNSS-based displacement estimation (blue).

A node is defined as the absolute position of each road agent, which is denoted as $\mathbf{X}_{a,t}$ for agent a at the tth epoch. The absolute position estimated by ray-tracing based 3DMA GNSS of each road agent is employed as a one-sided constraint using the red edge, which is denoted as $\hat{\mathbf{X}}_{a,t}$. The green edge is defined as the constraint of relative position between the different agents, which is denoted as $\Delta\mathbf{X}_{ab,t}$ for that between agents a and b at epoch t. The blue edge is defined as the displacement constraint between the different epochs of a road agent, which is denoted as $\Delta\mathbf{X}_{a,t\to t+1}$ for agent a from epochs t to $t+1$. By expanding the graph with new estimated constraints, the graph can be updated. Hence, the overall optimal positioning solution of each road agent can be obtained based on optimizing the graph. Since the position of each agent is determined considering all the available constraints, through space and time, the estimated solution is hence more accurate and robust against errors comparing to the anchor based approach [37].

B. Uncertainty Evaluation During Factor Graph Optimization

The reliability of each constraint is essential. Simply using the DOP of the GNSS measurement cannot describe the uncertainty of GNSS solution, especially in the case of urban canyons. The DOP value could be untrustworthily small due to severely affected NLOS receptions. We previously proposed to use the predicted positioning error map (shown in Fig. 2) to identify the friendliness of the environment that GNSS receivers located [53]. Previously, we used this approach to find the "anchor" of the collaborative system. In other words, it is a binary classification, healthy and not healthy. In this paper, we use the predicted GNSS error as the uncertainty of the edges (constraints). The predicted error map (PEM) can be regarded as a function to obtain the predicted error of a position $\mathbf{x_a}$ on the map.

$$\mathrm{PEM}\,(\mathbf{x_a}) = \begin{bmatrix} \mathrm{err}_{\mathbf{x_a}}^{east} \\ \mathrm{err}_{\mathbf{x_a}}^{north} \end{bmatrix} \quad (13)$$

where $\mathrm{err}_{\mathbf{x_a}}^{east}$ denotes the positioning error in the east direction based on $\mathbf{x_a}$. The $\mathbf{x_a}$ is estimated by the ray-tracing based 3DMA GNSS [39] in this paper. However, $\mathbf{x_a}$ may contain errors. To deal with this uncertainty, we propose to include

Authorized licensed use limited to: Hong Kong Polytechnic University. Downloaded on July 27,2023 at 10:24:04 UTC from IEEE Xplore. Restrictions apply.

more grids, $\mathbf{P}_{\mathbf{x_a}}^{err}$, within a certain radius $r = 10$ meters around $\mathbf{x_a}$. This value is heuristically determined by the uncertainty of $\mathbf{x_a}$. Thus, the predict error sets of the selected grids along east and north directions can be expressed as:

$$\begin{bmatrix} \mathrm{err}_{\mathbf{x_a}}^{east} \\ \mathrm{err}_{\mathbf{x_a}}^{north} \end{bmatrix} = \left\{ \mathrm{PEM}\left(\mathbf{P}_{\mathbf{x_a}}^{err}\right) \mid \left\| \mathbf{P}_{\mathbf{x_a}}^{err} - \mathbf{x_a} \right\| \leq r \right\} \tag{14}$$

Finally, the noise covariance matrix of the absolute position $\mathbf{x_a}$ is given by:

$$\Omega_{\mathbf{x_a}}^{\mathbf{abs}} = \begin{bmatrix} \left(\bar{\mathrm{err}}_{\mathbf{x_a}}^{east}\right)^2 & \mathbf{0} \\ \mathbf{0} & \left(\bar{\mathrm{err}}_{\mathbf{x_a}}^{north}\right)^2 \end{bmatrix} \tag{15}$$

where $\bar{}$ denotes the average calculation. Similarly, the noise covariance matrix of the relative position between road agents a and $b\,\Delta\hat{x}_{ab}$ is given by:

$$\Omega_{\Delta\hat{\mathbf{X}}_{ab}}^{rel} = \begin{bmatrix} \left(\bar{\mathrm{err}}_{\mathbf{x_a}}^{east}\right)^2 + \left(\bar{\mathrm{err}}_{\mathbf{x_b}}^{east}\right)^2 & 0 \\ 0 & \left(\bar{\mathrm{err}}_{\mathbf{x_a}}^{north}\right)^2 + \left(\bar{\mathrm{err}}_{\mathbf{x_b}}^{north}\right)^2 \end{bmatrix} \tag{16}$$

For the constraint of the displacement of a road agent, the uncertainty should be decided based on the behavior of road agents.

$$\Omega_{\mathbf{x_a},t\to t+1}^{displacement} = \begin{bmatrix} \sigma_{a,t\to t+1} & \mathbf{0} \\ \mathbf{0} & \sigma_{a,t\to t+1} \end{bmatrix} \tag{17}$$

where $\sigma_{a,t\to t+1}$ denotes the uncertainty of a road agent between two epochs. The behavior can be intelligently detected based on the classifier trained by machine learning or deep learning approaches. An example using raw sensor data of smartphones to detect the behavior can be found [54]. A similar approach can be used to classify whether the road agent is a pedestrian or a road vehicle. This paper selects $\sigma_{a,t\to t+1} = 0.2$ meter because the experiments are done by pedestrians. After defining the constraints and corresponding uncertainties in the graph, we have to minimize the cost of factors.

C. Optimization of the Constructed Factor Graph

The objective function is constructed by the cost of each factor mentioned earlier. The cost of the absolute position is defined as follows:

$$\varepsilon_{a,t} = \mathbf{H}(\mathbf{x}_{a,t}) - \hat{\mathbf{x}}_{a,t} \tag{18}$$

$\varepsilon_{a,t}$ is the cost for the absolute positioning constraint for road agent a at epoch t. Transform matrix $\mathbf{H}$ is the identity matrix. The cost function for the constraint of relative position between different road agents at the same epoch:

$$\varepsilon_{ab,t} = \mathbf{H}\left(\mathbf{x}_{b,t}\right) - \mathbf{H}\left(\mathbf{x}_{a,t}\right) - \Delta\hat{\mathbf{x}}_{ab,t} \tag{19}$$

where $\varepsilon_{ab,t}$ is the cost vector regarding the relative constraint between the different road agents a and b at the same epoch t. $\Delta\hat{x}_{ab,t}$ is calculated based on (12). The cost of the constraint of a road agent's displacement from time epochs t and $t+1$ is derived by:

$$\varepsilon_{a,t\to t+1} = \mathbf{H}\left(\mathbf{x}_{a,t+1}\right) - \mathbf{H}\left(\mathbf{x}_{a,t}\right) - \Delta\hat{\mathbf{x}}_{a,t\to t+1} \tag{20}$$

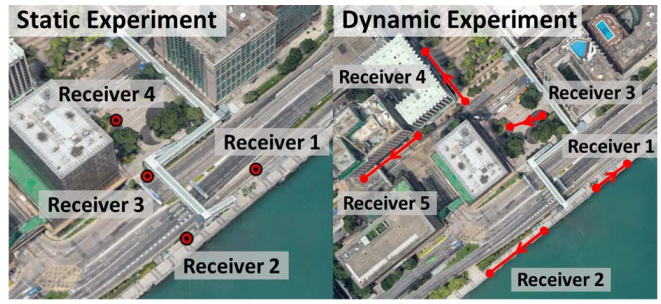

Fig. 8. Experimental design: static (left) and dynamic (right) experiments with 4 and 5 receivers, respectively.

where $\Delta\hat{\mathbf{x}}_{a,t\to t+1}$ denotes the displacement of a road agent, which is calculated using the equations below:

$$\Delta\hat{\mathbf{x}}_{a,t\to t+1} = \hat{\mathbf{v}}_{a,t} \cdot \Delta t \tag{21}$$

$$\hat{\mathbf{v}}_{a,t} = \left(\mathbf{G}^{\mathbf{T}}\mathbf{G}\right)^{-1}\mathbf{G}^{\mathbf{T}}\mathbf{f}_{a,t} \tag{22}$$

where $\hat{\mathbf{v}}_{a,t}$ denotes the estimated velocity of agent a using the measured GNSS Doppler frequency $\mathbf{f}_{a,t}$ (after correcting satellite clock drift). $\mathbf{G}$ denotes the unit LOS matrix. Finally, the objective function for this FGO is defined as:

$$\chi^* = \arg\min_{\chi} \sum_k \|\varepsilon_k\|^2_{\Omega_{\mathbf{k}}^{-1}} \tag{23}$$

where $\chi = \left[\mathbf{x}_1 \cdots \mathbf{x}_N\right]^{\mathrm{T}}$ is the vector of the N nodes in the graph and χ^* is the optimized position of each node. ε_k is the cost for the kth constraint, where $\varepsilon_{a,t}, \varepsilon_{ab,t}, \varepsilon_{a,t\to t+1} \in \varepsilon_k$. $\mathbf{\Omega_k}$ is the noise covariance matrix with the corresponding uncertainty constraint which can be found in (15, 16 and 17). By employing the Levenberg-Marquardt optimization method [46], the optimal positions of each road agent can be achieved with higher accuracy and robustness.

V. Experiment Results and Discussions

A. Experiment Setup

Static and dynamic experiments are conducted in urban canyons in Hong Kong as shown in Fig. 8. We use pedestrian to replace the vehicle as the data collection platform. Consumer-grade GNSS receiver, ublox M8T, is selected since it is popular in the ITS field. GNSS receivers are simultaneously collecting raw measurements in NMEA and RINEX format, with the sampling rate as 1Hz. The GNSS measurements are synchronized based on the GPS time and post-processed on the MATLAB programming platform. The ground truth of this experiment is obtained by comparing the landmark in Google Earth. We compare the following approaches:

1) LS: Conventional least square method,
2) RT: Ray-tracing based 3DMA GNSS [39],
3) SDM-CP: SDM 3DMA GNSS using anchor based collaborative method [37],
4) RT-CP: Ray-tracing 3DMA GNSS using anchor based collaborative method,
5) SDM-FGO: Apply FGO to SDM-CP, and
6) RT-FGO (proposed method): Apply FGO to RT-CP

Authorized licensed use limited to: Hong Kong Polytechnic University. Downloaded on July 27,2023 at 10:24:04 UTC from IEEE Xplore. Restrictions apply.

TABLE I
COMPARISON BETWEEN EXPERIMENTAL AND PREDICTED GPS POSITIONING ERRORS

Receiver No.	1	2	3	4
LS Positioning Error (m)	3.7	5.0	14.7	30.9
Predicted Mean Error (m)	3.1	2.9	6.6	16.3
Operating Status	Healthy	Healthy	Degraded	Degraded

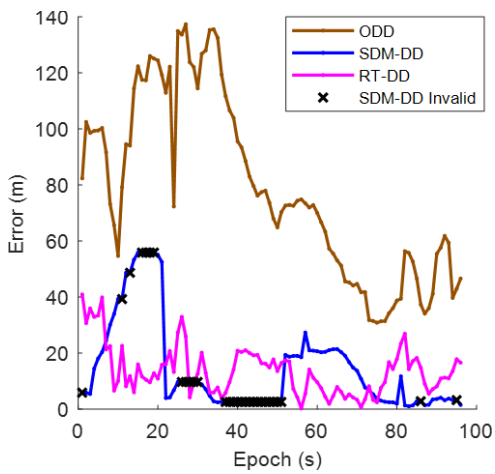

Fig. 9. The error of the relative positioning estimation between Receivers 1 and 4 based on the conventional double difference (DD), the shadow matching visibility-based double difference (SDM-DD) [37] and the proposed grid based 3DMA GNSS relative positioning (RT-DD). The black cross denotes the epoch when the SDM-DD was unable to provide a valid solution (SDM-DD Invalid).

TABLE II
THE RMSES, MAX ERRORS AND AVAILABILITY OF THE RELATIVE POSITIONING SOLUTIONS FROM DIFFERENT METHODS

Method	DD	SDM-DD	RT-DD
RMSE (m)	84.6	20.3	16.3
Max error (m)	137.4	55.8	40.9
Availability	100%	70%	100%

B. Static Experimental Results

The comparison between experimental and predicted GPS positioning errors of each receiver is given in Table I. Since the ray-tracing simulation cannot perfectly model the receiver noise and other error factors, the simulated error may lower than the actual GNSS error that receiver experienced.

The errors of the relative position between receivers estimated by different approaches are shown in Fig. 9. The corresponding root mean square errors (RMSEs) and maximum errors (Max errors) are shown in Table II. The Receiver 4 suffered from multipath effects and NLOS receptions. Although the conventional DD method can eliminate common errors, it is very sensitive to the multipath effect and NLOS reception. As a result, its relative positioning error is enormous with an RMSE of 84.6 m. One idea is to exclude the NLOS measurements before the DD process. Our previous work uses the satellite visibility determined by shadow matching (SDM) to exclude the NLOS ones [37]. Thereby, its estimated relative position is improved comparing to the conventional DD. However, the available LOS signal is limited in urban areas, thus making the surviving measurements after the SDM exclusion also limited. Due to the unsatisfactory satellite distribution of the surviving measurement, the SDM-DD has an RMSE of 20.3 m for the relative positioning. Moreover, the amount of surviving measurements may even be insufficient for positioning, thus making the availability of the valid SDM-DD solution only 70%. Using the proposed grid based 3DMA GNSS relative positioning, the reflected GNSS measurements are corrected instead of excluded. As a result, the relative positioning accuracy is further improved comparing to our previous work, the SDM-DD method, reaching an RMSE of 16.3 m.

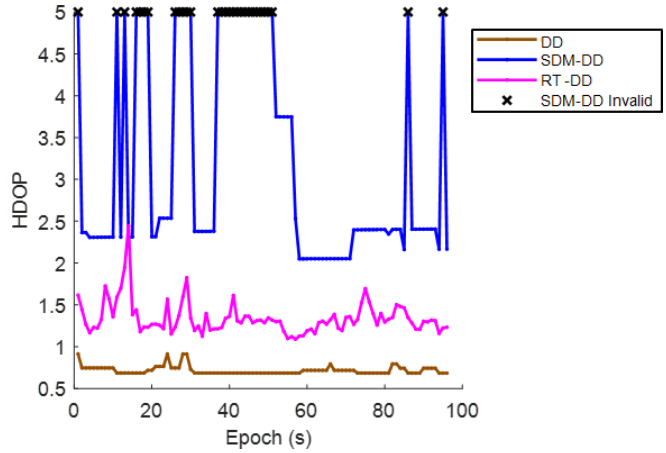

Fig. 10. The HDOP of the DD, SDM-DD and RT-DD.

The benefit of applying the proposed 3DMA GNSS relative positioning can be further explained by comparing the horizontal DOP (HDOP) of the used DD measurements as shown in Fig. 10.

The mean of the HDOP of the original DD measurement (nor exclusion or correction) is about 0.72. Using the satellite visibility of SDM to exclude the NLOS measurement, the HDOP increases to a mean of 2.41. By using the ray-tracing correction, the HDOP is maintained as 1.34 in average, which enables the RT-DD to achieve a better relative positioning solution. The reason of the HDOP of RT-DD higher than that of DD is RT cannot also correct NLOS if the reflected route is not detected.

After obtaining the relative position between Receivers 4 (degraded) and 1 (healthy), the absolute position of Receiver 4 can be collaboratively estimated based on the idea of our previous work [37]. By employing Receiver 1 as an accurate anchor, the absolute position of Receiver 4 (RT-CP) can be computed using the absolute position of Receiver 1 and the proposed grid based 3DMA GNSS relative positioning between Receivers 1 and 4. The errors of different anchor based collaborative positioning methods are shown in Fig. 11. The conventional LS obtains a performance of 30.9 m in RSME. The SDM approach excludes NLOS measurements, therefore improving the positioning accuracy to RMSE of 16.2 meters with 70% availability. The proposed

Authorized licensed use limited to: Hong Kong Polytechnic University. Downloaded on July 27,2023 at 10:24:04 UTC from IEEE Xplore. Restrictions apply.

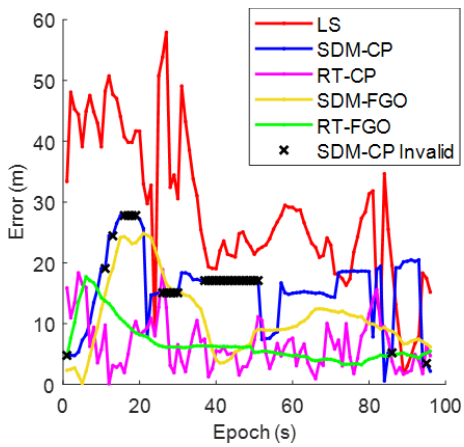

Fig. 11. The error of absolute positioning of receiver 4 by LS, SDM-CP, RT-CP, SDM-FGO and RT-FGO.

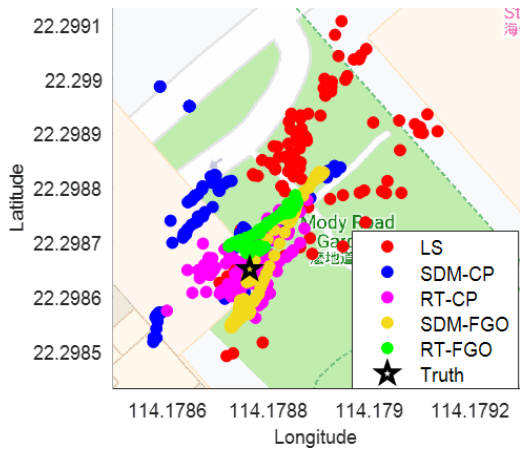

Fig. 12. The absolute positioning solutions of receiver 4 by LS, SDM-CP, RT-CP, SDM-FGO, RT-FGO and the ground truth.

grid based 3DMA GNSS relative positioning uses ray-tracing correction and collaborates with an anchor receiver, generating an improved performance of 7.8 m in RMSE, which is nearly three times better than that of the conventional LS method.

However, the RT-CP method conducts positioning based on a single anchor, which is not always reliable. In some of the epochs, both the relative position from the double difference and the absolute position from the ray-tracing 3DMA GNSS of Receivers 1 and 4 may not be accurate, thus resulting in the positions being inaccurate in these epochs. As Fig. 11 shows, the positioning error distribution of RT-CP is largely fluctuated. To improve the robustness of the collaborative positioning, we use the FGO considering all the constraints mentioned in Section IV and the result is shown in Fig. 12.

Using the factor graph optimization for the SDM-CP, some of the positions with enormous errors are reduced by the constraints during optimization. Comparing with SDM-FGO, the proposed method (RT-FGO) highly reduces the RMSE from 12.6 m to 7.4 m and the Max error from 24.8 m to 17.7 m. As shown in Fig. 12, the positioning solution of the proposed method (green) is more accurate and precise compared to other methods.

In addition to Receiver 4, the positioning accuracy of the participating receivers are improved by RT-FGO as shown in Table III. The proposed method achieves the best performance, which is three times better than that of the LS. The proposed method also largely improves the result from the stand-alone ray-tracing 3DMA GNSS [39]. Although the improvement of the RT-FGO compared to the RT-CP is only 0.4 m with respect to the RMSE, the robustness of the positioning solution is improved. For another degraded receiver (Receiver 3), the single-anchor-based RT-CP method slightly improves the positioning accuracy with respect to the other methods by nearly 2 m in the RMSE. By using the factor graph optimization, the positioning accuracy is significantly improved to an RMSE of 8.4 m. Moreover, comparing with the anchor-based RT-CP method, the peak error is remarkably reduced from 25.8 m to 11.7 m after applying the proposed collaborative optimization with other users. Since the optimization obtains an overall optimal solution and the uncertainty of the constraints may not be very accurate, the positioning solution of the healthy receiver after optimization may be slightly degraded compared to other methods. In general, the proposed 3DMA GNSS-based collaborative positioning algorithm with factor graph optimization is able to achieve an overall more accurate and robust positioning solution with an RMSE of less than 10 m for each receiver in the urban areas.

TABLE III

THE RMSE (MAX ERROR) IN METERS OF ABSOLUTE POSITIONING OF EACH RECEIVER USING DIFFERENT APPROACHES

Receiver No.	1	2	3	4
LS	3.7 (5.9)	5.0 (15.3)	14.7 (20.9)	30.9 (57.9)
RT	2.7 (4.3)	3.1 (5.4)	14.9 (33.8)	10.4 (17.9)
SDM-CP	4.2 (10.5)	4.7 (8.8)	14.2 (20.8)	16.2 (27.8)
RT-CP	2.3 (4.1)	3.5 (5.4)	12.5 (25.8)	7.8 (18.9)
SDM-FGO	2.3 (5.0)	2.6 (5.3)	14.7 (18.7)	12.6 (24.8)
RT-FGO	2.7 (5.0)	4.1 (5.5)	8.4 (11.7)	7.4 (17.7)

C. Dynamic Experimental Results

The relative positioning errors of different methods, including all Receivers and operating epochs, are compared in terms of the RMSE and Max error in Table IV as well as the cumulative distribution functions (CDFs) in Fig. 13. Since the differential approach can worsen the multipath and NLOS effects, most of the conventional DD estimation results contain enormous errors. The SDM-DD excludes the NLOS measurement achieving an improved relative positioning result that 69% of the errors are within 10 m. Note that Receiver 5 is located on a narrow street with two-side tall surface buildings, the NLOS reception is severe and the number of direct

Authorized licensed use limited to: Hong Kong Polytechnic University. Downloaded on July 27,2023 at 10:24:04 UTC from IEEE Xplore. Restrictions apply.

TABLE IV
THE RELATIVE POSITIONING RMSE (MAX ERROR) IN METERS BETWEEN RECEIVERS IN THE DYNAMIC EXPERIMENT

Between Receivers	R1-R2	R1-R3	R2-R3	R1-R4	R2-R4	R3-R4	R1-R5	R2-R5	R3-R5	R4-R5
DD	5.2 (10.9)	82.4 (201.8)	82.0 (202.4)	51.4 (104.1)	52.9 (109.4)	68.9 (206.5)	103.2 (166.1)	102.4 (170.2)	85.2 (158.9)	85.4 (158.8)
SDM-DD	4.3 (9.6)	8.7 (45.8)	8.8 (52.1)	7.7 (36.1)	6.1 (18.8)	6.0 (17.1)	29.0 (120.4)	21.8 (67.0)	20.8 (29.0)	48.1 (131.1)
RT-DD	4.3 (10.1)	4.5 (9.7)	3.1 (11.1)	3.6 (11.0)	4.0 (14.3)	6.0 (19.3)	20.2 (40.1)	20.9 (39.4)	20.8 (31.8)	23.7 (37.9)

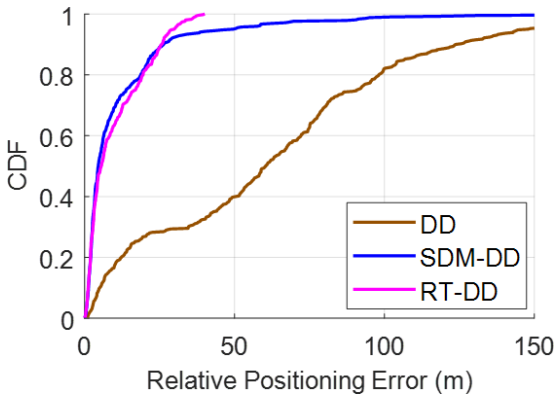

Fig. 13. The relative positioning error CDFs of the conventional DD, SDM-DD and the proposed RT-DD for all the Receivers and all epochs.

GNSS signals is very limited. Due to the lack of common satellites in view (as we demonstrated in Fig. 1), the SDM-DD relative position performance between Receiver 5 and other receivers is significantly degraded, leading to 6% of the error exceeds 40 m. By employing the complementary characteristic between the ray-tracing algorithm and the double difference method, the relative positioning accuracy can be further improved. Comparing to SDM-DD, RT-DD ensures a sufficient amount of measurements, which mitigates the enormous relative positioning errors to below 40 m, achieving a much lower Max error. Specifically, the relative positioning RMSEs between Receiver 3, 4 and 5 are all below 6 m. Notice that the relative positioning error of R3-R4 is larger than R1-R4 or R2-R4. It is probably because the ray-tracing technique cannot completely correct all the NLOS errors, which makes the measurement noise after correction is still higher than the open-sky scenario. Therefore, collaborating with the road agents from healthy scenarios could enhance the potential for better performance. However, for Receiver 5 located in a narrow street, the measurements are possibly experiencing double reflections, which is not considered in our NLOS correction. Therefore, the proposed grid based 3DMA GNSS relative positioning is unable to achieve satisfactory performance for Receiver 5.

For Receivers 3, 4 and 5 that located in a dense urban area, the positioning results of the proposed and other collaborative positioning methods are shown in Fig. 14 (a), (b) and (c), respectively. For the Receivers 3 and 4, the anchor-base cooperative positioning method (RT-CP) can achieve a better positioning solution comparing to conventional methods. Using the FGO, all the available measurements are used as constraints for the global optimal solution. The optimized solutions from SDM-FGO and RT-FGO are more robust and closer to the true position. The performances of the proposed and other methods are evaluated with RMSE and Max error in Table V.

For Receivers 1 and 2 which located in the GNSS-friendly environment, the proposed algorithm can maintain their performance during the optimization. For Receivers 3 and 4 located in a dense urban area, the accurate relative positions are used to improve the positioning accuracy with RT-CP, achieving the RMSE twice lower than the LS method and 3 meters better than stand-alone RT method. By applying with FGO, the positioning accuracy of Receiver 4 is improved within 5 meters of RMSE. Interestingly, the optimized solution for Receiver 3 is not better than the RT-CP method, which is due to the improper uncertainty of the constraint of the displacement in FGO. Since the Doppler measurement is not accurate for Receiver 3 and is given a smaller uncertainty, the solutions may drift and resulting additional 2 meters in RMSE. As mentioned earlier, the proposed NLOS correction method may not be able to fully correct the double reflected signal delay by only considering single reflection. Then, the remnant delay could degrade the positioning performance, may even worse than the exclusion-based method. Therefore, the RMSE of the proposed method achieves a performance of 18.6 meters in RMSE. Comparing to receiver's NMEA position result with sophisticated filtering techniques, our proposed method can achieve significant improvements for most of the scenarios. In general, the proposed 3DMA GNSS collaborative positioning method with factor graph optimization can significantly improve the GNSS positioning accuracy in dense urban areas.

D. Noise Analysis

To evaluate the benefit of our proposed method, the GNSS measurement noise during the collaborative positioning is analyzed. The GNSS measurement noise combines with systematic error and uncommon error. The systematic error is eliminated by the DD method. For the urban scenario, the majority of the uncommon error is the NLOS delay, which can be corrected by the RT method. Then, the remaining noise required to be analyzed is the RT correction residual.

The GNSS pseudorange error CDFs before and after RT correction during the dynamic experiment are compared in Fig. 15. The pseudorange error is estimated using double differential measurements with the knowledge of the ground truth location [55]. Most of the NLOS errors are corrected by

Authorized licensed use limited to: Hong Kong Polytechnic University. Downloaded on July 27,2023 at 10:24:04 UTC from IEEE Xplore. Restrictions apply.

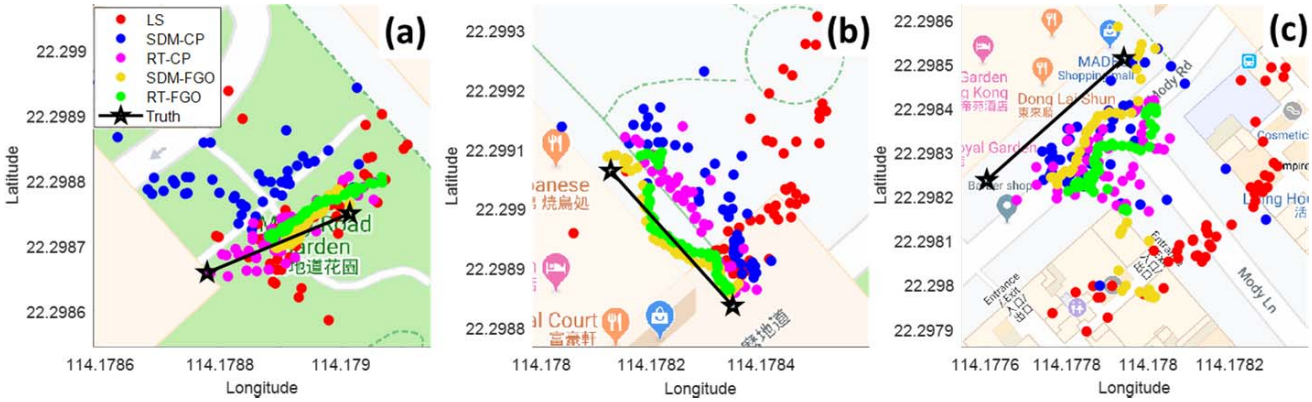

Fig. 14. The positioning results of the proposed 3DMA GNSS based collaboative positioning with factor graph optimization (RT-FGO) comparing to that of the conventional least square method (LS), shadow matching based cooperative positioning method (SDM-CP), anchor-based positioning method using ray-tracing (RT-CP) and SDM based cooperative positioning with factor graph optimization (SDM-FGO) for the receiver 3 (a), receiver 4 (b) and receiver 5 (c) in dense urban areas.

TABLE V
THE ABSOLUTE POSITIONING RMSE (MAX ERROR) IN METERS OF EACH RECEIVER IN THE DYNAMIC EXPERIMENT

Receiver No.	R1	R2	R3	R4	R5
LS	4.3 (9.3)	2.0 (4.0)	14.6 (33.7)	25.3 (48.1)	46.5 (52.3)
NMEA	1.2 (2.1)	5.4 (6.6)	13.5 (17.7)	10.6 (15.4)	27.6 (31.7)
RT	5.1 (10.3)	3.1 (12.8)	8.5 (21.4)	10.6 (23.8)	20.1 (35.3)
SDM-CP	4.9 (9.8)	2.4 (4.7)	14.7 (33.6)	12.0 (27.7)	18.3 (66.8)
RT-CP	5.4 (9.5)	2.5 (6.4)	5.3 (14.7)	7.6 (16.3)	19.3 (35.1)
SDM-FGO	5.6 (11.3)	1.7 (3.0)	7.5 (12.8)	3.4 (5.3)	25.5 (50.8)
RT-FGO	5.1 (9.5)	2.1 (3.5)	8.1 (12.8)	4.2 (9.4)	18.6 (30.3)

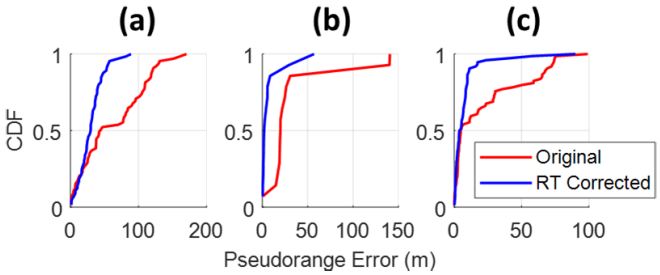

Fig. 15. The GNSS pseudorange error CDFs before and after ray-tracing corrections for Receiver 3 (a), Receiver 4 (b) and Receiver 5 (c) during the dynamic experiment.

the RT method, which significantly reduces the pseudorange error comparing to the original measurement. Note that a few measurements still have the correction residual over 50 meters. It is due to the double reflection or diffraction effect that cannot be modelled by the RT method.

To evaluate the impact of the correction residual, we analyze the likelihood distribution used to determine the relative position (as described in Section III). The averaged likelihood

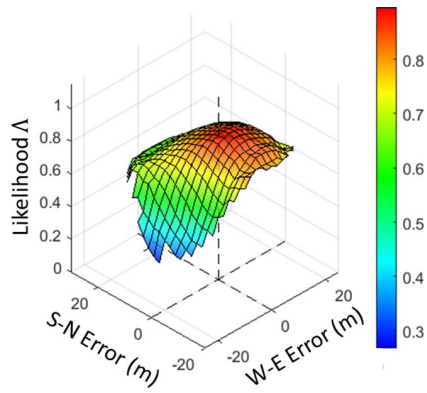

Fig. 16. The averaged likelihood distribution for each grid pair during the proposed relative positioning between Receivers 3 and 4. S-N Error and W-E Error denote the error between the relative grid position and the true relative position on the South-North or West-East directions. The likelihood value is indicated with height and color.

distribution among all the grid pairs during the relative positioning between Receivers 3 and 4 is shown as Fig. 16. For each pair of grids, its relative grid position vector is compared with the actual relative position between Receivers, to estimate the West-East (W-E) and South-North (S-N) errors. Afterward, the likelihood values of all pairs are constructed as a likelihood distribution corresponding to the W-E and S-N error. Then, the likelihood distributions of all epochs during operation will be averaged, representing the overall performance. Since the likelihood distributions may not always have the same coverage on "W-E error" and "S-N error", only the area with over ten epochs occurrence will be considered.

From the averaged likelihood distribution, the highest peak is located close to the coordinates (0,0). On the contrary, the likelihood value significantly decreased for the pairs with higher error. Although the RT correction remains residual, the RT corrected DD estimation from the correct pair is still consistent with the actual Receivers relative position, achieving a high likelihood value. Therefore, the impact of the correction residual is sufficiently low, which guarantees the likelihood value on the correct pair much higher than that on the fault pair. By using the likelihood values as weights, the pairs with higher likelihood will have more contribution in the

Authorized licensed use limited to: Hong Kong Polytechnic University. Downloaded on July 27,2023 at 10:24:04 UTC from IEEE Xplore. Restrictions apply.

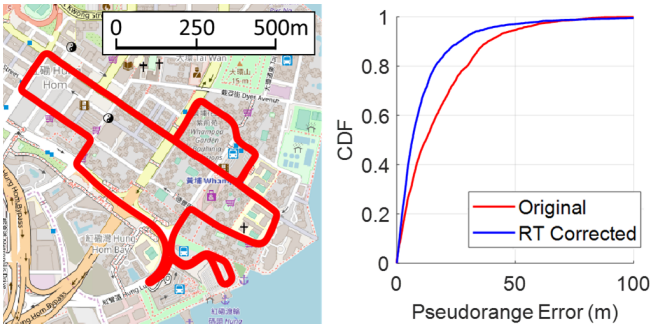

Fig. 17. (Left) The clock-wise vehicular experiment route in the urban scenario. (Right) The CDFs of pseudorange errors before and after applying the ray-tracing correction.

proposed method, which enables us to estimate the relative position with lower W-E and S-N error.

Since the dynamic experiment is conducted with limited scenarios, an additional vehicular experiment is conducted to evaluate the RT correction residual for various scenarios. As Fig. 17 (left) shows, the vehicle is driven with a clock-wise route in an urban area of Hong Kong. There are 2895 epochs (1Hz) in total. The true position of the vehicle is obtained by the Novatel SPAN-CPT with the real-time kinematic solution. The CDFs of pseudorange error before and after applying the RT correction are shown in Fig. 17 (right). The proposed RT method can correct most of the NLOS delays, achieving 80% of the pseudorange errors are less than 16.3 m, much lower than the original 29.7 m. However, there still exist 15% of the pseudorange errors exceed 20 m after correction. This could come from we mistakenly apply the RT correction to a diffracted-pseudorange measurement or a double-reflected-pseudorange measurement.

VI. Conclusion and Future Work

In this study, a centralized 3DMA GNSS-based collaborative positioning algorithm using factor graph optimization is proposed to improve the positioning accuracy of the participated road agents in dense urban areas. By applying the ray-tracing algorithm to correct the NLOS delay caused by buildings, the uncommon errors between different receivers are mitigated. Then, the remaining systematic GNSS errors can be eliminated using the double difference technique. Based on their complementary characteristic, the ray-tracing and double difference combined method can achieve a more accurate relative positioning.

By employing the receiver located in GNSS-friendly area as an anchor for collaborative positioning, the positioning accuracy of the degraded receiver is significantly improved to an RMSE of 7.8 m with the proposed method, while the conventional LS achieves 30.9 m. By further applying the FGO, all the available measurements are used to enhance the robustness of the positioning solution, achieving an RMSE of less than 10 m for most of the participating road agents in the dense urban area.

However, the ray-tracing algorithm simulates the GNSS signal reflecting point by searching every building surface using every grid for all the received satellites, which is proved too computational costly for a single user [56]. Additionally, the pair-wise evaluation will enhance the computation load in a squared way. For practical applications, it is necessary to reduce the computation load in the future, for example, using a unique pre-generated storage format [57] or utilizing a simplified ray-tracing method [56]. Moreover, the uncertainty of the constraint estimated from the positioning error map may not be stable or accurate, which is another challenge that needs to be solved in the future.

On the other hand, although a large network size could help to scale down the variance of noisy factors [58], merely increasing the number of collaborators may not be an optimal approach. Some adjacent road agents in the same area may have similar NLOS effects. Meanwhile, some of the agents may have complementary positioning error ellipsoids, due to different surrounding buildings or satellite visibilities. It has great potential to better improve the positioning performance by intelligently selecting the collaborating agents based on their characteristics. However, this requires detail and large-scale analysis with a realistic simulator considering all possible effects. Therefore, the development of realistic simulator and intelligent collaborator selection will also be the future works. With appropriate agent reliability estimation and the intelligent collaborator selection, the large-scale experimental evaluation could be practically conducted based on smartphones using low-cost GNSS chip.

References

[1] F. de Ponte Müller, "Survey on ranging sensors and cooperative techniques for relative positioning of vehicles," *Sensors*, vol. 17, no. 2, p. 271, 2017.

[2] N. Alam and A. G. Dempster, "Cooperative positioning for vehicular networks: Facts and future," *IEEE Trans. Intell. Transp. Syst.*, vol. 14, no. 4, pp. 1708–1717, Dec. 2013.

[3] S. Bhamidipati and G. X. Gao, "GPS multireceiver joint direct time estimation and spoofer localization," *IEEE Trans. Aerosp. Electron. Syst.*, vol. 55, no. 4, pp. 1907–1919, Aug. 2019.

[4] G. M. Hoang, B. Denis, J. Harri, and D. T. M. Slock, "Cooperative localization in GNSS-aided VANETs with accurate IR-UWB range measurements," in *Proc. 13th Workshop Positioning, Navigat. Commun. (WPNC)*, Oct. 2016, pp. 1–6.

[5] J. Liu, B.-G. Cai, and J. Wang, "Cooperative localization of connected vehicles: Integrating GNSS with DSRC using a robust cubature Kalman filter," *IEEE Trans. Intell. Transp. Syst.*, vol. 18, no. 8, pp. 2111–2125, Aug. 2017.

[6] M. Elazab, A. Noureldin, and H. S. Hassanein, "Integrated cooperative localization for vehicular networks with partial GPS access in Urban Canyons," *Veh. Commun.*, vol. 9, pp. 242–253, Jul. 2017.

[7] A. Minetto, C. Cristodaro, and F. Dovis, "A collaborative method for positioning based on GNSS inter agent range estimation," in *Proc. 25th Eur. Signal Process. Conf. (EUSIPCO)*, Aug. 2017, pp. 2714–2718.

[8] D. Yang, F. Zhao, K. Liu, H. B. Lim, E. Frazzoli, and D. Rus, "A GPS pseudorange based cooperative vehicular distance measurement technique," in *Proc. IEEE 75th Veh. Technol. Conf. (VTC Spring)*, May 2012, pp. 1–5.

[9] F. de Ponte Müller, E. M. Diaz, B. Kloiber, and T. Strang, "Bayesian cooperative relative vehicle positioning using pseudorange differences," in *Proc. IEEE/ION Position, Location Navigat. Symp. PLANS*, May 2014, pp. 434–444.

[10] N. Alam, A. T. Balaei, and A. G. Dempster, "Relative positioning enhancement in VANETs: A tight integration approach," *IEEE Trans. Intell. Transp. Syst.*, vol. 14, no. 1, pp. 47–55, Mar. 2013.

[11] K. Liu, H. B. Lim, E. Frazzoli, H. Ji, and V. C. S. Lee, "Improving positioning accuracy using GPS pseudorange measurements for cooperative vehicular localization," *IEEE Trans. Veh. Technol.*, vol. 63, no. 6, pp. 2544–2556, Jul. 2014.

Authorized licensed use limited to: Hong Kong Polytechnic University. Downloaded on July 27,2023 at 10:24:04 UTC from IEEE Xplore. Restrictions apply.

[12] A. Minetto, A. Nardin, and F. Dovis, "Tight integration of GNSS measurements and GNSS-based collaborative virtual ranging," in *Proc. 31st Int. Tech. Meeting Satell. Division Inst. Navigat. (ION GNSS+)*, Miami, Florida, Oct. 2018, pp. 2399–2413.

[13] N. Alam, A. T. Balaei, and A. G. Dempster, "Positioning enhancement with double differencing and DSRC," in *Proc. ION GNSS*, Sep. 2010, pp. 20–24.

[14] K. Lassoued, P. Bonnifait, and I. Fantoni, "Cooperative localization with reliable confidence domains between vehicles sharing GNSS pseudoranges errors with no base station," *IEEE Intell. Transp. Syst. Mag.*, vol. 9, no. 1, pp. 22–34, Jan. 2017.

[15] N. Zhu, J. Marais, D. Betaille, and M. Berbineau, "GNSS position integrity in urban environments: A review of literature," *IEEE Trans. Intell. Transp. Syst.*, vol. 19, no. 9, pp. 2762–2778, Sep. 2018.

[16] L.-T. Hsu, "Analysis and modeling GPS NLOS effect in highly urbanized area," *GPS Solutions*, vol. 22, no. 1, p. 7, Jan. 2018.

[17] S. Godha and M. E. Cannon, "GPS/MEMS INS integrated system for navigation in urban areas," *GPS Solutions*, vol. 11, no. 3, pp. 193–203, May 2007.

[18] C. Hide and T. Moore, "GPS and low cost INS integration for positioning in the urban environment," in *Proc. ION GPS*, Sep. 2005, pp. 13–16.

[19] G. Zhang and L.-T. Hsu, "Intelligent GNSS/INS integrated navigation system for a commercial UAV flight control system," *Aerosp. Sci. Technol.*, vol. 80, pp. 368–380, Sep. 2018.

[20] A. Fascista, G. Ciccarese, A. Coluccia, and G. Ricci, "Angle of arrival-based cooperative positioning for smart vehicles," *IEEE Trans. Intell. Transp. Syst.*, vol. 19, no. 9, pp. 2880–2892, Sep. 2018.

[21] G. De Angelis, A. De Angelis, V. Pasku, A. Moschitta, and P. Carbone, "An experimental system for tightly coupled integration of GPS and AC magnetic positioning," *IEEE Trans. Instrum. Meas.*, vol. 65, no. 5, pp. 1232–1241, May 2016.

[22] G. De Angelis, G. Baruffa, and S. Cacopardi, "GNSS/Cellular hybrid positioning system for mobile users in urban scenarios," *IEEE Trans. Intell. Transp. Syst.*, vol. 14, no. 1, pp. 313–321, Mar. 2013.

[23] Z. M. Kassas and T. E. Humphreys, "Observability analysis of collaborative opportunistic navigation with pseudorange measurements," *IEEE Trans. Intell. Transp. Syst.*, vol. 15, no. 1, pp. 260–273, Feb. 2014.

[24] P. D. Groves and M. Adjrad, "Performance assessment of 3D–mapping–aided GNSS—Part 1: Algorithms, user equipment, and review," *Navigation*, vol. 66, no. 2, pp. 341–362, Jun. 2019.

[25] L.-T. Hsu, Y. Gu, and S. Kamijo, "3D building model-based pedestrian positioning method using GPS/GLONASS/QZSS and its reliability calculation," *GPS Solutions*, vol. 20, no. 3, pp. 413–428, Jul. 2016.

[26] T. Suzuki and N. Kubo, "GNSS positioning with multipath simulation using 3D surface model in urban canyon," in *Proc. 25th Int. Tech. Meeting Satell. Division Inst. Navigat. (ION GNSS)*, Dec. 2012, pp. 438–447.

[27] T. Suzuki and N. Kubo, "Correcting GNSS multipath errors using a 3D surface model and particle filter," in *Proc. ION (GNSS+)*, Sep. 2013, pp. 16–20.

[28] N. I. Ziedan, "Urban positioning accuracy enhancement utilizing 3D buildings model and accelerated ray tracing algorithm," in *Proc. 30th Int. Tech. Meeting Satell. Division Inst. Navigat. (ION GNSS+)*, Portland, Oregon, Nov. 2017, pp. 3253–3268.

[29] L. Wang, P. D. Groves, and M. K. Ziebart, "Smartphone shadow matching for better cross-street GNSS positioning in urban environments," *J. Navigat.*, vol. 68, no. 3, pp. 411–433, May 2015.

[30] P. D. Groves and M. Adjrad, "Likelihood-based GNSS positioning using LOS/NLOS predictions from 3D mapping and pseudoranges," *GPS Solutions*, vol. 21, no. 4, pp. 1805–1816, Oct. 2017.

[31] P. D. Groves, "Shadow matching: A new GNSS positioning technique for urban canyons," *J. Navigat.*, vol. 64, no. 3, pp. 417–430, Jul. 2011.

[32] L. Wang, P. D. Groves, and M. K. Ziebart, "GNSS shadow matching: Improving urban positioning accuracy using a 3D city model with optimized visibility scoring scheme," *Navigation*, vol. 60, no. 3, pp. 195–207, Sep. 2013.

[33] R. Yozevitch and B. B. Moshe, "A robust shadow matching algorithm forGNSSPositioning," *Navigation*, vol. 62, no. 2, pp. 95–109, Sep. 2015.

[34] M. Adjrad, P. D. Groves, J. C. Quick, and C. Ellul, "Performance assessment of 3D–mapping–aided GNSS—Part 2: Environment and mapping," *Navigation*, vol. 66, no. 2, pp. 363–383, Jun. 2019.

[35] S. Tanwar and G. X. Gao, "Decentralized collaborative localization in urban environments using 3D-Mapping-Aided (3DMA) GNSS and inter-agent ranging," in *Proc. 31st Int. Tech. Meeting Satell. Division Inst. Navigat. (ION GNSS+)*, Oct. 2018, pp. 2352–2363.

[36] A. Conti, M. Guerra, D. Dardari, N. Decarli, and M. Z. Win, "Network experimentation for cooperative localization," *IEEE J. Sel. Areas Commun.*, vol. 30, no. 2, pp. 467–475, Feb. 2012.

[37] G. Zhang, W. Wen, and L.-T. Hsu, "Rectification of GNSS-based collaborative positioning using 3D building models in urban areas," *GPS Solutions*, vol. 23, no. 3, p. 83, Jul. 2019.

[38] G. Zhang, W. Wen, and L.-T. Hsu, "A novel GNSS based V2 V cooperative localization to exclude multipath effect using consistency checks," in *Proc. IEEE/ION Position, Location Navigat. Symp. (PLANS)*, Apr. 2018, pp. 1465–1472.

[39] S. Miura, L.-T. Hsu, F. Chen, and S. Kamijo, "GPS error correction with pseudorange evaluation using three-dimensional maps," *IEEE Trans. Intell. Transp. Syst.*, vol. 16, no. 6, pp. 3104–3115, Dec. 2015.

[40] M. Obst, S. Bauer, and G. Wanielik, "Urban multipath detection and mitigation with dynamic 3D maps for reliable land vehicle localization," in *Proc. IEEE/ION Position, Location Navigat. Symp.*, Apr. 2012, pp. 685–691.

[41] A. Howard, M. J. Matark, and G. S. Sukhatme, "Localization for mobile robot teams using maximum likelihood estimation," in *Proc. IEEE/RSJ Int. Conf. Intell. Robots Syst.*, Sep. 2002, pp. 434–439.

[42] P. Oguz-Ekim, J. Gomes, J. Xavier, and P. Oliveira, "A convex relaxation for approximate maximum-likelihood 2D source localization from range measurements," in *Proc. IEEE Int. Conf. Acoust., Speech Signal Process.*, Mar. 2010, pp. 2698–2701.

[43] T. V. Nguyen, Y. Jeong, H. Shin, and M. Z. Win, "Least square cooperative localization," *IEEE Trans. Veh. Technol.*, vol. 64, no. 4, pp. 1318–1330, Apr. 2015.

[44] F. Wickelmaier, "An introduction to MDS," *Sound Qual. Res. Unit, Aalborg Univ., Denmark*, vol. 46, no. 5, pp. 1–26, May 2003.

[45] M. Efatmaneshnik, A. T. Balaei, N. Alam, and A. G. Dempster, "A modified multidimensional scaling with embedded particle filter algorithm for cooperative positioning of vehicular networks," in *Proc. IEEE Int. Conf. Veh. Electron. Saf. (ICVES)*, Nov. 2009, pp. 7–12.

[46] F. Dellaert, *Factor Graphs and GTSAM: A Hands-on Introduction*. Atlanta, Georgia: Georgia Institute of Technology, 2012.

[47] M. Kaess, H. Johannsson, R. Roberts, V. Ila, J. J. Leonard, and F. Dellaert, "ISAM2: Incremental smoothing and mapping using the Bayes tree," *Int. J. Robot. Res.*, vol. 31, no. 2, pp. 216–235, Feb. 2012.

[48] R. M. Watson and J. N. Gross, "Robust navigation in GNSS degraded environment using graph optimization," in *Proc. 30th Int. Tech. Meeting Satell. Division Inst. Navigat. (ION GNSS+)*, Portland, Oregon, Nov. 2017, pp. 1–8.

[49] W. Wen, Y. C. Kan, and L.-T. Hsu, "Performance comparison of GNSS/INS integrations based on EKF and factor graph optimization," in *Proc. 32nd Int. Tech. Meeting Satell. Division Inst. Navigat. (ION GNSS+)*, Miami, Florida, Oct. 2019, pp. 3019–3032.

[50] G. Zhang and L.-T. Hsu, "A new path planning algorithm using a GNSS localization error map for UAVs in an urban area," *J. Intell. Robotic Syst.*, vol. 94, no. 1, pp. 219–235, Apr. 2019.

[51] N. Alam, A. T. Balaei, and A. G. Dempster, "Positioning enhancement with double Differencing and DSRC," in *Proc. 23rd Int. Tech. Meeting Satell. Division The Inst. Navigat. (ION GNSS)*, Portland, Oregon, Sep. 2010, pp. 1210–1218.

[52] E. Kaplan and C. Hegarty, *Understanding GPS: Principles and Applications*. Norwood, MA, USA: Artech House, 2005.

[53] G. Zhang, W. Wen, and L.-T. Hsu, "Collaborative GNSS positioning with the aids of 3D city models," in *Proc. 31st Int. Tech. Meeting Satell. Division Inst. Navigat. (ION GNSS+)*, Miami, Florida, Oct. 2018, pp. 143–149.

[54] H. Gao and P. D. Groves, "Environmental context detection for adaptive navigation using GNSS measurements from a smartphone," *Navigation*, vol. 65, no. 1, pp. 99–116, Mar. 2018.

[55] Xu, Jia, Luo, and Hsu, "Intelligent GPS l1 LOS/Multipath/NLOS classifiers based on Correlator-, RINEX- and NMEA-level measurements," *Remote Sens.*, vol. 11, no. 16, p. 1851, 2019.

[56] H. F. Ng, G. Zhang, and L.-T. Hsu, "Range-based 3D mapping aided GNSS with NLOS correction based on skyplot with building boundaries," in *Proc. ION Pacific PNT Meeting*, Honolulu, HI, USA, May 2019, pp. 8–11.

[57] X. Liu, S. Nath, and R. Govindan, "Gnome: A practical approach to NLOS mitigation for GPS positioning in smartphones," in *Proc. 16th Annu. Int. Conf. Mobile Syst., Appl., Services*, Jun. 2018, pp. 163–177.

[58] M. Pirani *et al.*, "Cooperative vehicle speed fault diagnosis and correction," *IEEE Trans. Intell. Transp. Syst.*, vol. 20, no. 2, pp. 783–789, Feb. 2019.

Authorized licensed use limited to: Hong Kong Polytechnic University. Downloaded on July 27,2023 at 10:24:04 UTC from IEEE Xplore. Restrictions apply.

Guohao Zhang received the bachelor's degree in mechanical engineering and automation from the University of Science and Technology, Beijing, China, in 2015, and the master's degree in mechanical engineering from The Hong Kong Polytechnic University, where he is currently pursuing the Ph.D. degree. His research interests including global navigation satellite system urban localization, collaborative positioning, and multisensor integrated navigation.

Hoi-Fung Ng received the Bachelor of Engineering degree (Hons.) in air transport engineering from the Interdisciplinary Division of Aeronautical and Aviation Engineering, The Hong Kong Polytechnic University, Hong Kong, in 2018. He is currently a Research Assistant with The Hong Kong Polytechnic University. His research interests include 3D mapping-aided global navigation satellite system localization and navigation.

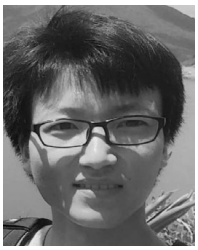

Weisong Wen was born in Ganzhou, Jiangxi, China. He is currently pursuing the Ph.D. degree in mechanical engineering with The Hong Kong Polytechnic University. He is also a Visiting Student Researcher with the University of California, Berkeley (UCB). His research interests include GNSS/INS/LiDAR/HD map-based localization for autonomous vehicles.

Li-Ta Hsu (Member, IEEE) received the B.S. and Ph.D. degrees in aeronautics and astronautics from National Cheng Kung University, Taiwan, in 2007 and 2013, respectively. He was a Post-Doctoral Researcher with the Institute of Industrial Science, The University of Tokyo, Japan. In 2012, he was a Visiting Scholar with University College London, U.K. He is currently an Assistant Professor with the Division of Aeronautical and Aviation Engineering, The Hong Kong Polytechnic University. He is also a Technical Representative with ION and an Associate Fellow with RIN. His research interests include global navigation satellite system positioning in challenging environments, localization for pedestrian, autonomous driving vehicle, and unmanned aerial vehicle.

Authorized licensed use limited to: Hong Kong Polytechnic University. Downloaded on July 27,2023 at 10:24:04 UTC from IEEE Xplore. Restrictions apply.